ENGINEERING

Ultrawideband dynamic microwave frequency-amplitude measurement

Huan He¹, Jingchuan Wang², Zhiyong Zhao¹*, Dongmei Huang², Alan Pak Tao Lau², Chao Lu², Ming Tang¹*

Microwave measurement is crucial in various fields, such as communication, radar, and cognitive radio, now poised for a revolution with the advent of photonic-assisted techniques that promise unprecedented performance. However, existing methods often disrupt the amplitude integrity of unknown signals and rely on time-consuming frequency sweeping to achieve multifrequency detection, which markedly restricts their instantaneous bandwidth, response speed, and accuracy. Here, we present a groundbreaking approach leveraging digital optical frequency comb-enabled stimulated Brillouin scattering to achieve instantaneous microwave frequency and amplitude detection, attaining a record-breaking 50.8-gigahertz bandwidth, a 1.1-megahertz accuracy, and a 500-nanosecond temporal resolution, which is three orders of magnitude improvement over that obtained with frequency sweeping schemes. In addition to conventional frequency detection, the proposed technique enables simultaneous multifrequency microwave amplitude measurement and achieves a substantial performance enhancement in the figure of merit of more than 10-fold, which paves the way for dynamic microwave signal detection and analysis.

Copyright © 2025 The Authors, some rights reserved; exclusive licensee American Association for the Advancement of Science. No claim to original U.S. Government Works. Distributed under a Creative Commons Attribution NonCommercial License 4.0 (CC BY-NC).

INTRODUCTION

Dynamic characterization of unknown microwave signals plays a pivotal role in a myriad of applications, encompassing high-speed communication, radar detection, satellite surveillance, and electronic intelligence (1-3). With the rapid development of microwave technology, the carrier frequencies of signals now span from hundreds of megahertz to hundreds of gigahertz, and diverse complicated modulation formats are widely used (4). However, traditional electrical measurement methods face substantial challenges due to limitations in analog-to-digital conversion rates and instantaneous electronic bandwidths and to severe frequency-dependent loss and electromagnetic interference (EMI) (5-7). In response, photonicassisted measurements have emerged as potent tools for frequency estimation, offering a wideband measurement range, a rapid response, and low loss, particularly in scenarios requiring remote, distributed, and EMI-resistant measurements (8-10). These systems aim to meet the urgent need for characterizing broadband signals beyond tens of gigahertz with nearly real-time measurement speeds.

Photonic-assisted solutions are typically categorized on the basis of the optical processes used to map an unknown frequency to the output power or time delay (11). First, frequency-power mapping schemes (12, 13), in which an amplitude comparison function related to the test frequency is established, often face a trade-off between the measurement range and accuracy (14–18), alongside power drift of key components, which limits the measurement accuracy to more than a few hundred megahertz (19). Moreover, these methods are only applicable to single-frequency measurements. In contrast, frequency-to-time mapping schemes provide a multifrequency measurement capability (20, 21). Using a dispersion-induced time delay, these schemes can identify multiple tone frequencies but suffer from poor spectral resolution, up to gigahertz (22). To increase the spectral

¹Wuhan National Lab for Optoelectronics (WNLO), School of Optical and Electronic Information, Huazhong University of Science and Technology, Wuhan 430074, China. ²Photonics Research Centre, Department of Electrical and Electronic Engineering, The Hong Kong Polytechnic University, Hong Kong, SAR, China.

*Corresponding author. Email: zhiyongzhao@hust.edu.cn (Z.Z.); tangming@mail. hust.edu.cn (M.T.)

resolution, various frequency scanning measurement systems have been proposed (23–26). Among them, schemes leveraging the stimulated Brillouin scattering (SBS) effect, which is characterized by a narrowband filter response, exhibit superior measurement accuracy and spectral resolution, typically within a few tens of megahertz (27–30).

However, the interrogation of narrowband Brillouin spectra relies on small-step frequency sweep operations, which are time consuming and thus severely limit the system measurement speed. Typically, thousands of frequency sweeps are needed to obtain a wide measurement range while maintaining the measurement accuracy, resulting in a temporal resolution of hundreds of microseconds or even longer (30). Recently, a scheme based on the optical chirp chain transient SBS effect was demonstrated to achieve a realtime response but with degraded spectral resolution and additional compensation algorithms (31, 32). In addition, the small instantaneous bandwidths of existing SBS-based schemes make realizing dynamic measurements over a large measurement range challenging. Furthermore, most photonic-assisted schemes can only perform instantaneous frequency identification, during which the amplitude information of unknown microwave signals is usually disrupted or destroyed, leading to incomplete characterization and thus limiting their practical application (33–35).

In this work, we propose and demonstrate an ultrawideband dynamic microwave signal measurement scheme using the digital optical frequency comb (DOFC)-enabled SBS effect. The broadband DOFC enables simultaneous measurement of all the Brillouin spectra generated by an unknown microwave signal within the probe bandwidth without frequency sweeping or extra distortion. A record instantaneous bandwidth of 50.8 GHz and a measurement accuracy of less than 1.1 MHz are achieved by leveraging the instantaneous complex information of Brillouin gain and loss. This superior dynamic performance, with a 500-ns temporal resolution, corresponds to an improvement of at least three orders of magnitude over that of conventional frequency sweeping schemes. Furthermore, the amplitude of the unknown microwave signal can also be detected via the SBS intensity, which allows dynamic measurements of amplitude-modulated signals with a multifrequency system. In the experiments,

the system exhibits a versatile ability to identify and quantify multifrequency signals and complex microwave signals, including frequency-modulated and amplitude-modulated microwave signals as well as their combinations. In addition, the measurement accuracy can be enhanced using synthetic measurements with extra Brillouin phase information. To evaluate the comprehensive performance, a figure of merit (FOM) is defined, and the proposed system outperforms the state-of-the-art method by a factor of more than 10, showing unprecedented potential for instantaneous frequency identification. Moreover, the ability to measure both frequency and amplitude paves the way for characterizing complex microwave signals in practical implementations.

RESULTS

Operating principle

Figure 1A illustrates the operating principle of the proposed instantaneous microwave signal measurement approach that uses the broadband DOFC-enabled SBS effect. The system relies on a pumpprobe configuration (36), in which the unknown microwave signal under test (SUT) with frequency f_s and amplitude a_s drives an electro-optical modulator to generate pump light with carriersuppressed double-sideband modulation in the remote unit, while a single sideband-modulated broadband DOFC serves as the probe. Unlike the traditional single-frequency probe, the DOFC features tens of thousands of multitone signals with uniform frequency spacing f_{rep} , which enables simultaneous capture of spectral information across a wide bandwidth, thus eliminating the need for timeconsuming frequency sweeping and markedly increasing the measurement speed. The pump light and backpropagating DOFC probe interact in the optical fiber with a specific Brillouin frequency shift (BFS), denoted as v_B . This interaction results in frequency-selective Brillouin amplification or attenuation within the DOFC probe bandwidth, thus allowing direct detection of the instantaneous Brillouin gain/loss and phase shift. Once the center frequency of the Brillouin spectrum is located, the frequency f_s of the SUT can be determined with the help of v_B . Moreover, the amplitude a_s of the SUT is proportional to the pump power, which affects the detected SBS intensity. Therefore, in addition to frequency detection, the proposed approach allows simultaneous demodulation of the amplitude information of the SUT, which has never been experimentally verified in previous schemes.

As shown in Fig. 1B, when the modulation bandwidth of the DOFC exceeds $2v_B$, the instantaneous bandwidth of the frequency measurement is defined by the starting frequency f_1 and ending frequency f_k of the DOFC baseband signal. To prevent the Brillouin gain cross-talk induced by the unwanted sideband of the modulated pump and avoid low-frequency noise due to self-heterodyning of the DOFC probe, we set the starting frequency f_1 to v_B . Thus, both the Brillouin gain spectrum (BGS) and Brillouin loss spectrum (BLS) are used to extend the frequency coverage. Within the bandwidth range of the received DOFC, only the BLS exists for $f_s < 2\nu_B$, whereas only the BGS exists for $f_s > f_k - v_B$. For $2v_B < f_s < f_k - v_B$, both the BLS and the BGS are present and can be used to determine the gain/loss peak. Assuming that the located center frequencies obtained for the BLS and BGS are f_g and f_l , respectively, the measured frequencies of the SUT derived from these two spectra are $f_s = f_g + v_B$ and $f_s = f_1 - v_B$, respectively. As a result, the frequency coverage used for microwave signal f_s identification ranges from 0 to $f_k + v_B$, indicating an extended instantaneous bandwidth that surpasses the DOFC modulation bandwidth by $2v_B$.

Dynamic measurements can be achieved by continuously launching the DOFC probe, with each DOFC frame sequentially capturing the SBS signal generated by the unknown microwave signal. These

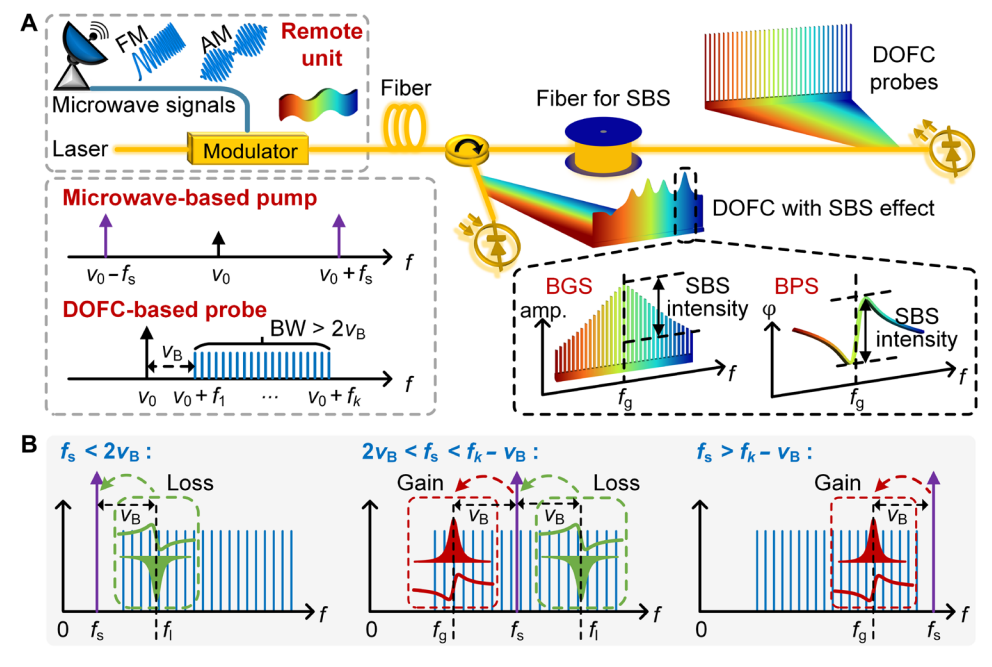


Fig. 1. Ultrawideband microwave signal measurement using the DOFC-enabled SBS effect. (**A**) Schematic of the microwave-modulated pump and DOFC-modulated probe, as well as the detected DOFC demodulated Brillouin spectrum. (**B**) Direct detection of the received DOFC spectrum in three SUT frequency ranges, including only the BLS for $f_s < 2v_B$, both the BLS and BGS for $2v_B < f_s < f_k - v_B$, and only the BGS for $f_s > f_k - v_B$. FM, frequency modulation; AM, amplitude modulation; BW, bandwidth.

Brillouin spectra are temporally encoded with the sampled SUT and converted into the measured frequencies through the BGS or BLS. At the same time, the amplitude of the SUT is mapped via the SBS intensity, thus enabling dynamic reconstruction of the SUT in terms of both its frequency and amplitude over time.

Experimental setup

Figure 2A depicts the experimental setup. A tunable narrow linewidth laser (NKT Koheras BASIK X15) operating at 1550.12 nm emits continuous-wave (CW) light, which is split into two paths to serve as the carriers for the probe and pump signals. In the upper path, the light is modulated by a dual-drive Mach-Zehnder modulator (DDMZM; EOSPACE Z-cut; 40 GHz) to implement singlesideband modulation with a carrier. The modulator is driven by the DOFC baseband signal generated by a four-channel arbitrary waveform generator (AWG; Keysight, M8194A). Here, a DOFC baseband signal with 15,000 tones, a 10.4-GHz starting frequency, and a 2-MHz frequency spacing is used, which corresponds to a duration of 500 ns. The modulated broadband DOFC probe, amplified to 17 dBm by an erbium-doped fiber amplifier (EDFA; Amonics, AEDFA-PA-35-B-FA), is then launched into a 50-m polarization-maintaining fiber (PMF) with a BFS of 10.4 GHz. In the lower path, the unknown SUT drives an MZM (iXblue, MXAN-LN-40) to generate a doublesideband pump with carrier suppression. To ensure the long-term stability of the modulated signal, the bias point of the used modulator is automatically locked by a modulator bias controller (PlugTech, MBC-MZM) to avoid bias drift noise. In the experiment, the unknown SUT is generated by a wideband microwave source generator (MSG) with frequency and amplitude modulation. The optical spectra of the DOFC probe and pump modulated by microwave signals of various frequencies are shown in Fig. 2B. The CW pump light is

amplified by another EDFA in automatic current control mode. Thus, the output pump power of the EDFA is proportional to the input optical power, which is determined by the amplitude of the SUT. To maximize the SBS interaction efficiency and mitigate polarization-dependent fluctuations, the polarization states of the probe light and the pump light must be aligned before they enter the PMF, which is achieved using polarization controllers in our system; in addition, the isolator and circulator placed after them are also polarization-maintaining to ensure stability. Notably, the EDFA setup and the PMF can be used in conventional SBS-based schemes to achieve stable linear mapping of the SUT amplitude to the SBS intensity. For dynamic measurements, DOFC probes with a 500-ns duration are repeatedly generated for sequential interaction with the pump light. The probe that carries the SBS gain/loss information is detected by a photodetector (PD; Finisar, BPDV2120R-VM-LP), and the generated electrical DOFC frames are captured by an oscilloscope (OSC; Keysight, UXR0804A) for further digital signal processing. The demodulated spectra of the received DOFC frames with SBS signals generated by different SUTs are shown in Fig. 2C, facilitating extraction of the corresponding Brillouin spectra. As a result, the proposed system ensures a temporal resolution of 500 ns per measurement cycle. The measurable frequency range is from 0 to 50.8 GHz, thus yielding an ultrawideband instantaneous bandwidth of 50.8 GHz. These unprecedented performance parameters allow wideband simultaneous measurements of multiple microwave signals with complex modulations.

Instantaneous frequency identification

To demonstrate the high-accuracy frequency identification capability of the proposed technique, the MSG (Keysight, E8257D) generates constant-frequency microwave signals as the SUT, whose frequency

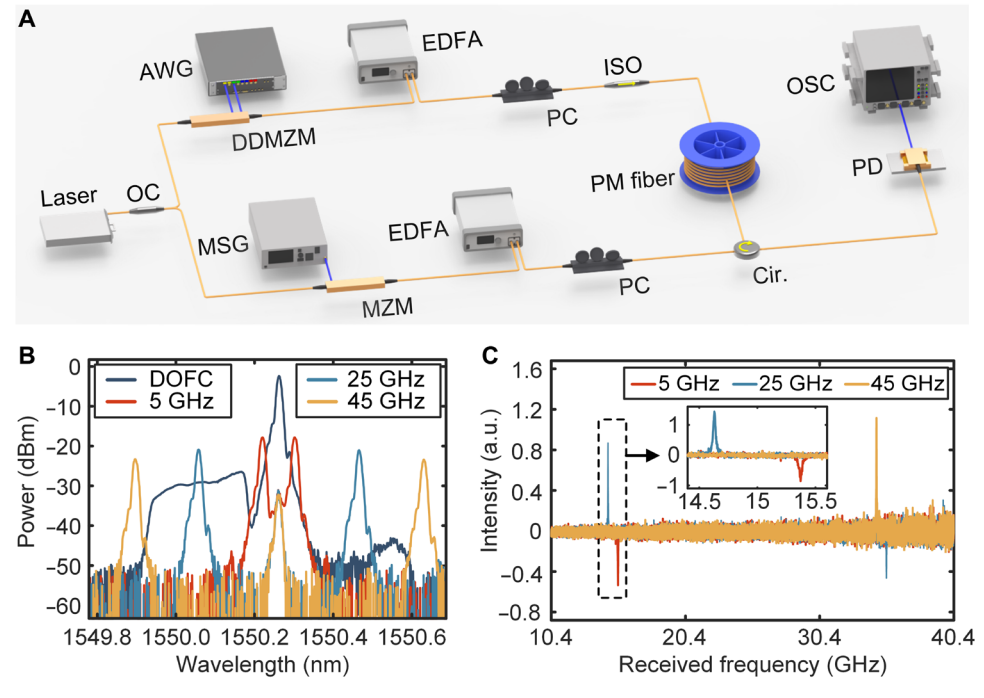


Fig. 2. Experimental setup. (A) Proposed microwave signal measurement system based on the DOFC-enabled SBS effect. (B) Optical spectra of the modulated DOFC probe and various pumps related to the SUT. (C) Demodulated DOFC spectra with the SBS signal generated by the SUT. OC, optical coupler; PC, polarization controller; ISO, optical isolator; Cir, optical circulator; a.u., arbitrary units.

ranges from 0.1 to 50 GHz with a 100-MHz increment. Without averaging, the amplitude and phase information of each frequency comb tone is obtained by applying a fast Fourier transform (FFT) to demodulate the pure Brillouin spectra within the received signal spectrum. For each DOFC frame, Lorentzian fitting is performed over the whole spectral range to capture the regions of the BGS and BLS, and the measured temporal evolutions of these spectra are depicted in Fig. 3 (A and B), respectively. To ensure optimal visualization of the relative intensity variations, the color scale bars in the results all indicate the normalized magnitude. Since the generated Brillouin spectra exhibit a 10.4-GHz frequency shift from the input SUT frequency, the BGS appears when the input SUT frequency exceeds 20.8 GHz, and the BLS within the received spectrum vanishes when the input SUT frequency exceeds 30 GHz. Notably, for input SUT frequencies between 20.8 and 30 GHz, both the BGS and BLS are detected and can, thus, be used for SUT measurement. However, although the BGS and BLS have opposite polarities, their frequency separation prevents amplitude aliasing via direct subtraction in the frequency domain for signal-to-noise ratio (SNR) enhancement. To use both spectra for microwave signal measurement, Lorentzian fitting needs to be applied separately to each spectrum to extract their respective center frequencies (37). Considering the computational complexity and that the gain spectrum tends to have a much higher SNR, the individual BGSs are preferred for SUT frequency measurements between 20.8 and 30 GHz in this demonstration. The center frequencies of these used Brillouin spectra are subsequently mapped to the actual frequencies, and, eventually, the various frequencies of the SUT can be individually identified.

Figure 3C displays the measured frequencies alongside the corresponding input frequencies, which verify the ability to accurately track the input frequency and exceed the 50-GHz instantaneous bandwidth of the proposed system. To evaluate the accuracy of the frequency measurement, we set the amplitude of the SUTs to 1 V over the entire frequency measurement range. One hundred repetitive experimental measurements are performed on the SUTs at each input frequency, and the measurement uncertainty is calculated as the root mean square error (RMSE) of the measured frequency. The uncertainty in the various frequency measurements extracted from the individual BLSs and BGSs is presented in Fig. 3D. Although the measurement accuracy decreases as the input frequency increases, the frequency uncertainty remains below 1.1 MHz over the detectable frequency range. Consequently, the system outperforms existing photonic-assisted schemes (20-30) in terms of instantaneous bandwidth and measurement accuracy, showing an unprecedented ability to recognize instantaneous frequencies. A detailed performance comparison is shown in the Performance Comparison section. Notably, the deterioration in the frequency uncertainty with increasing frequency is caused by the limited SNR of the high-frequency component of the received spectrum, and lower and flatter measurement uncertainties can be achieved later via DOFC baseband signal preequalization and optical power optimization. In addition, the SUT amplitude directly affects the SBS intensity, and a low SUT amplitude results in a low SNR, which also degrades the measurement accuracy. Therefore, maintaining an appropriate SUT amplitude range is critical for achieving accurate frequency measurements.

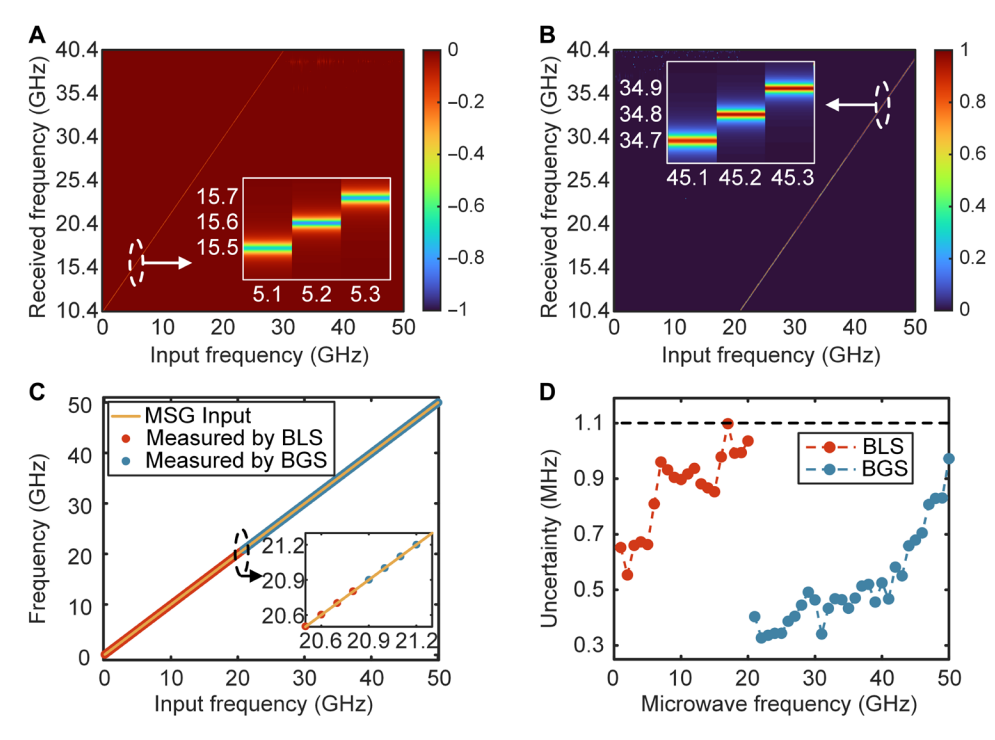


Fig. 3. Results of single-frequency microwave signal measurements. (A) Captured fitted BLSs and (B) BGSs over the received DOFC bandwidth range when the frequency of the SUT changes from 0.1 to 50 GHz at a step of 100 MHz. The insets show three 500-ns measurements with 100-MHz frequency steps for better observation. (C) Comparison of the stepped input frequency generated by the MSG and the measured frequencies independently demodulated based on the BLS and BGS. The inset shows a transition in the Brillouin spectrum at ~20.8 GHz. (D) Frequency measurement uncertainty calculated from 100 experimental measurements versus the input frequency with a step increase of 1 GHz.

Frequency-modulated microwave signal measurement

To assess the dynamic measurement capability, we generate various microwave signals with continuously changing frequencies using the frequency modulation module of the MSG (Keysight, N5183B). Initially, the SUT has a sinusoidal frequency modulated at ~19.5 GHz, which falls within the frequency measurement range with the worst accuracy, as shown in Fig. 3D. Figure 4A illustrates the temporal BLSs acquired for dynamic tracking of a 100-kHz sinusoidal signal with a 500-ns temporal resolution. The center position of the BLSs sinusoidally varies with the instantaneous SUT frequency, and the measured frequencies are presented in Fig. 4B. Despite this frequency range having the worst measurement accuracy, the measured temporal traces well match the time-varying input frequencies, demonstrating the robust dynamic tracking capability of the proposed system. Notably, the continuous frequency-modulated SUT drives the pump light, causing its frequency to change within the 500-ns response time of the SBS interaction. When the pump frequency rapidly changes, the SBS process cannot reach a steady state. This transient distortion leads to broadening of the Brillouin spectrum and a reduction in the measured SBS intensity, which becomes particularly pronounced at high frequency modulation rates, as shown in Fig. 4A. Furthermore, since linear frequency modulation and frequency-hopping microwave signals are crucial in modern radar and wireless communication, measurements of both types of frequency-modulated SUTs are also conducted to verify the feasibility. One type involves triangular waveform modulation, in which the frequency is linearly swept up and down over a 50-µs period. The other type involves encoding of a pseudorandom binary sequence of order 7 (PRBS7) with a bit rate of 500 kHz, which is a common test code in communication applications. As shown in Fig.

4 (C and D), the measured BGS evolution effectively validates the ability to dynamically track the triangle-modulated signal and the PRBS7-encoded signal with the proposed system.

To verify the ultrawide instantaneous bandwidth, we generate a frequency-agile SUT with a frequency from 5 to 40 GHz in 5-GHz steps using one channel of the AWG used and show the demodulated DOFC spectra of the SUT with different frequencies in Fig. 4E. The frequencies independently demodulated with the BLS and BGS after Lorentzian fitting are presented in Fig. 4F, where the difference between the demodulated and input frequencies represents the measurement error; these results show that the system can dynamically track the frequency-agile microwave signal over a wide bandwidth. With 15,000 frequency components contained in a single measurement cycle, the DOFC-based system achieves a temporal resolution of 500 ns, which is at least three orders of magnitude better than that of conventional frequency sweep-based schemes (30), ensuring an outstanding wideband high-precision dynamic multiple microwave frequency measurement capability.

Amplitude-modulated microwave signal measurement

In addition to dynamic frequency identification, the proposed scheme can also measure the amplitude of unknown microwave signals, which is typically not feasible with conventional schemes. Since the pump power depends on the input microwave amplitude and the SBS intensity is proportional to the pump power, the SUT amplitude can be estimated by measuring the SBS intensity. As a proof of concept, the input amplitude of a single-frequency microwave signal is varied between 0.5 and 1 V. Figure 5A displays the measured BGS evolution when the input microwave amplitude is

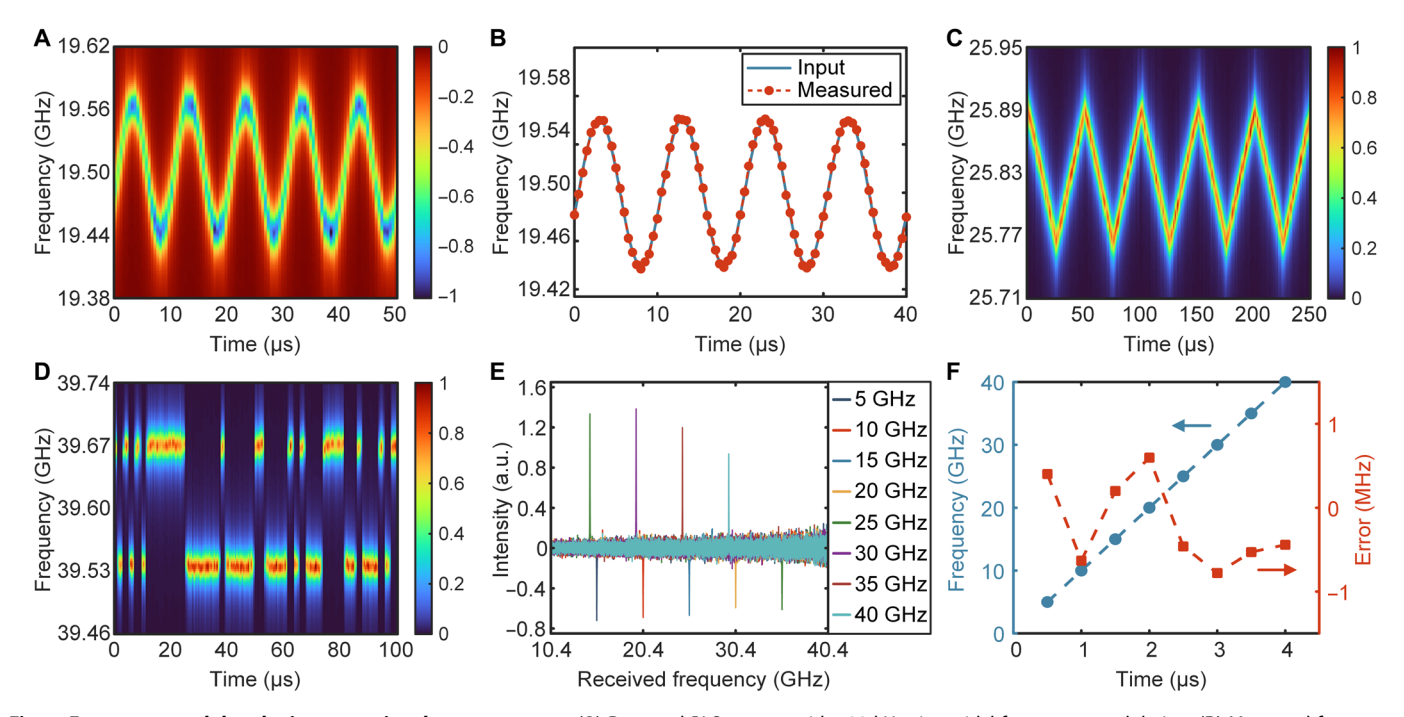


Fig. 4. Frequency-modulated microwave signal measurements. (A) Detected BLS spectra with 100-kHz sinusoidal frequency modulation. (B) Measured frequency variation under 100-kHz sinusoidal modulation. (C) Measured BGSs generated by a chirped microwave signal with a 20-kHz triangular modulation frequency. (D) Measured BGSs generated by the 500-kHz PRBS7 code with hopping frequencies. (E) Demodulated DOFC spectra when the frequency of the SUT changes from 5 to 40 GHz at a step of 5 GHz. (F) Measured frequency and its measurement error compared with the input frequency.

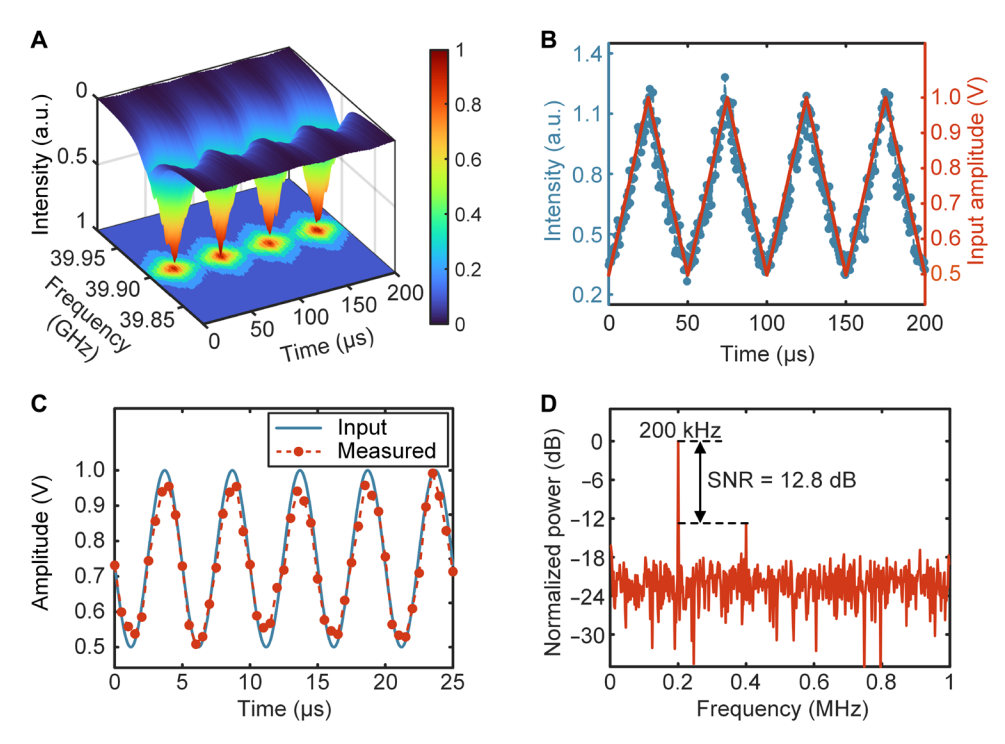


Fig. 5. Amplitude-modulated microwave signal measurements. (A) Evolution of the detected BGSs generated by a 20-kHz triangular amplitude modulation signal. (B) Measured SBS intensity of the amplitude-modulated SUT under 20-kHz triangular modulation. (C) Comparisons of the measured amplitude and the input amplitude of a 19.5-GHz SUT with 200-kHz sinusoidal amplitude modulation. (D) Power spectrum of the measured amplitude variation.

modulated with a 20-kHz triangular signal. Unlike frequency modulation, the amplitude modulation of the SUT results in a variation in the SBS intensity, whereas the center frequency of the BGS remains unchanged. The measured evolution of the SBS intensity is shown in Fig. 5B, which reveals an excellent linear dependence with respect to the input microwave amplitude. Thus, this linear dependence between the input and output verifies the feasibility of dynamically measuring the microwave amplitude at each frequency. Notably, both the minimum detectable amplitude and the resolution of the amplitude measurements are determined mainly by the noise floor of the received DOFC spectrum and the SBS interaction efficiency. The resolution of the amplitude measurement can be calculated on the basis of the variations observed during continuous amplitude measurements of a single-frequency signal with a constant amplitude. In this system, the minimum detectable amplitude of the system is ~0.2 V. Below this threshold, the SBS intensity becomes comparable to the background noise, leading to substantial measurement uncertainties. To analyze the accuracy of the dynamic amplitude measurements, we set the frequency of the SUT to 19.5 GHz, with a poor SNR, and modulate its amplitude by a 200-kHz sinusoidal waveform. Figure 5C presents the detected amplitude of the 19.5-GHz SUT obtained using the BLS, and the power spectrum of the demodulated amplitude is shown in Fig. 5D. The 200-kHz modulation frequency is clearly distinguished, with a high SNR of 12.8 dB, verifying the accurate dynamic measurement ability of the system for nonlinear amplitude modulated signals. Therefore, measurements of amplitude-modulated microwave signals are successfully demonstrated with a multifrequency measurement scheme, which will substantially enhance the ability to characterize microwave signals.

Complex microwave signal measurement

The dynamic detection capabilities of the proposed system for detecting the frequency and amplitude of unknown microwave signals have been individually demonstrated. To further investigate the system performance in detecting complex microwave signals, we use an SUT with both frequency modulation and amplitude modulation for experiments, and the fastest frequency switching time of the MSG used is ~230 ns for frequency modulation. Figure 6A displays the measured BGSs generated by a complex microwave signal with simultaneous 20-kHz sawtooth wave-frequency modulation and 100-kHz triangular wave-amplitude modulation. The SBS intensity exhibits five periodic variations during a single frequency modulation period. The measured SUT frequencies and amplitudes derived from the evolution of the BGS are shown in Fig. 6B.

The results confirm that the system can identify the instantaneous frequency while remaining unaffected by the amplitude modulation, ensuring accurate capture of frequency transitions. In addition, the demodulated signal amplitude based on the SBS intensity also well matches the amplitude of the SUT, with slight distortion caused by noise fluctuations in the DOFC spectrum, which directly affects the Lorentzian fitting of the BGS/BLS peak intensity. In contrast, the frequency measurement, which relies on fitting of the BGS/BLS peak position, is more robust to noise because of the symmetry of the Brillouin spectrum and its steep phase transition. The results verify the unparalleled ability of the proposed technique to accurately measure both the frequency and amplitude of any microwave signal with complex modulation formats, which is unattainable with previous schemes. This breakthrough heralds an unprecedented dimension in the characterization of microwave signals, setting a benchmark for future explorations.

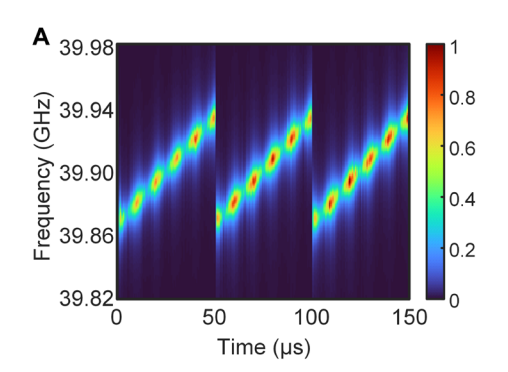
DISCUSSION

Spectral resolution for multifrequency microwave signals

The spectral resolution is a critical parameter for multifrequency measurements and denotes the minimum frequency difference that can be discerned. In SBS-based schemes, the spectral resolution is primarily limited by the linewidth of the measured Brillouin spectrum and the power ratio of the adjacent pump frequencies (38, 39). On the one hand, an excessively high power ratio complicates the identification of a frequency component with a lower power. On the other hand, as the frequency interval of the unknown multifrequency signals gradually decreases, the Brillouin spectra overlap; as a result, measurement inaccuracies or even errors can occur. Notably, the detected SNRs of the Brillouin spectra differ at distinct frequencies

within the DOFC bandwidth, which affects the Brillouin linewidth. For example, Lorentzian fitting reveals that the linewidths of the BLS from a 5-GHz SUT and the BGS from a 25-GHz SUT are 30.5 and 24.9 MHz, respectively, as illustrated in Fig. 7A. To systematically evaluate the Brillouin linewidths across the whole 50.8-GHz frequency range, 100 repetitive measurements with a 1-GHz interval are conducted for individual frequencies. As depicted in Fig. 7B, the Brillouin linewidths consistently remain below 32.7 MHz, and the maximum appears at 46 GHz.

Therefore, to analyze the spectral resolution of the proposed system for multifrequency microwave signal measurements, another MSG is used to generate an SUT with two frequencies around 46 GHz. The generated SUT consists of a constant frequency and a time-varying



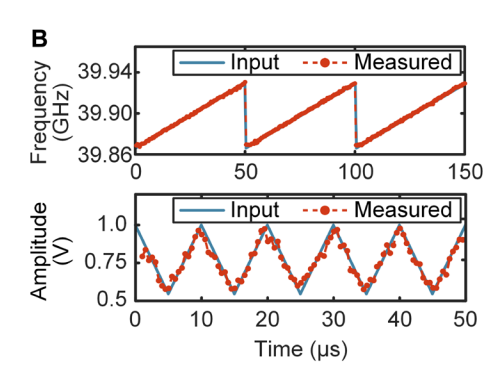


Fig. 6. Complex microwave signal measurements. (A) Detected Brillouin spectra generated by a complex SUT with 20-kHz sawtooth frequency modulation and 100-kHz triangular amplitude modulation. (B) The top graph shows the measured frequency of the complex SUT, and the bottom graph shows the measured amplitude during a single frequency modulation period.

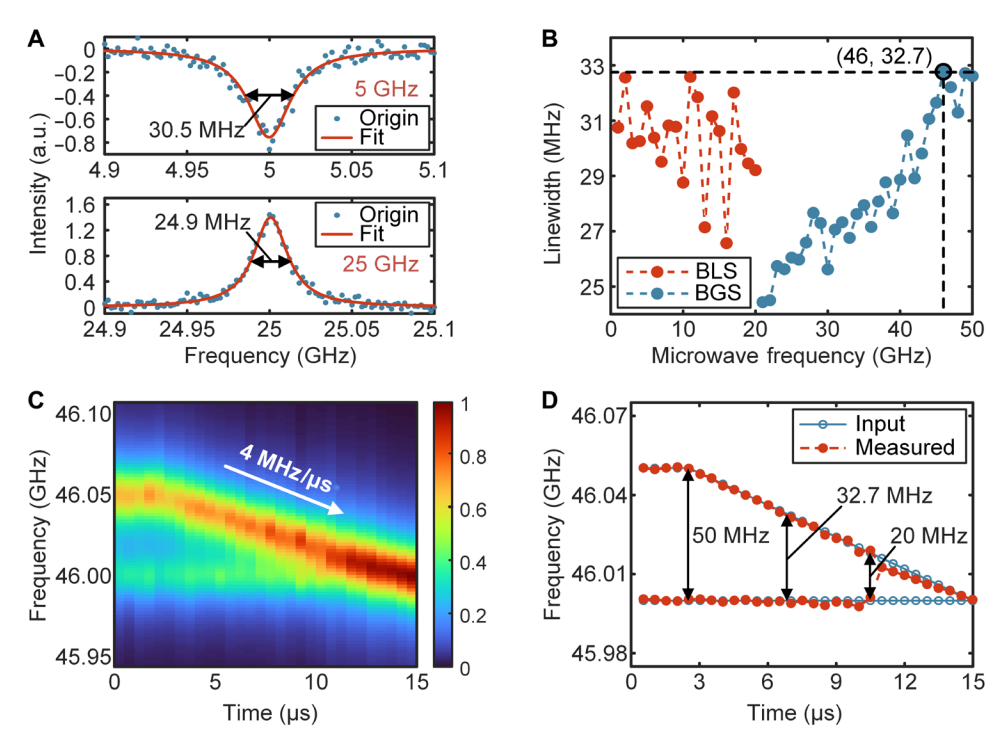


Fig. 7. Statistical analysis of the Brillouin spectral linewidth and multifrequency microwave signal measurements. (A) Detected original and fitted data of the BLS and BGS for different SUTs. (B) Measured Brillouin linewidths over a 50.8-GHz instantaneous bandwidth. (C) Measured BGS evolution of an SUT that contains a constant frequency of 46 GHz and a frequency that varies from 46.05 to 46 GHz. (D) Comparison of the measured frequencies and the input frequencies.

frequency to adjust their frequency interval, and their amplitudes are set to 0.5 and 1 V, respectively, to obtain a high power ratio. Here, the time-varying frequency component remains constant for the first 2.5 μs, after which its frequency linearly decreases until it reaches the same frequency as the other frequency component. Figure 7 (C and D) displays the recovered Brillouin spectra and the measured frequencies, respectively, which reveal a spectral aliasing phenomenon. When the interval between the two frequencies exceeds 20 MHz, the two frequencies of the SUT are still distinctly identifiable, although there are small fluctuations in the measurements when the interval is below the 32.7-MHz Brillouin linewidth. However, as the two frequencies approach each other, the Brillouin spectra become severely aliased and indistinguishable. Consequently, the results indicate that the proposed system has a high spectral resolution of 20 MHz over the entire measurement range.

In addition, for multifrequency signals with a measurement frequency difference close to 20.8 GHz, the BGS of the high-frequency tones overlaps with the BLS of the low-frequency tones, which complicates the spectral separation. For further performance enhancement, a multifrequency pump modulation technique can be considered to expand the nonaliasing bandwidth in the future (27).

Accuracy improvement via synthetic measurements

DOFC technology allows simultaneous and straightforward acquisition of the BGS, BLS, and Brillouin phase shift spectrum (BPS) (40). Since the BGS and BLS are susceptible to intensity noise, which consequently reduces the measurement accuracy for the SUT amplitude, more precise amplitude measurements can be obtained using the more noise-tolerant BPS. By using the same experimentally received data as those for the previously mentioned 200-kHz amplitude-modulated signal, the BPS is obtained, as shown in Fig. 8A. The inset shows the SBS intensity variation measured using the BPS, where the SNR calculated via the power spectrum is 13.8 dB, which is 1 dB higher than that obtained using the BGS. Notably, relying solely on a single Brillouin spectrum might compromise the accurate determination of the center frequency of the Brillouin spectrum because of the 2-MHz frequency resolution and received noise. Hence, to improve the frequency measurement accuracy, averaging the measured frequencies from the BLS/BGS and BPS to determine the final measurement frequency is advisable. As illustrated in Fig. 8B, a comparison of the frequency uncertainties obtained using different spectrum data, including the individual BGS, the individual BPS, and their combination, is presented. These results indicate that comparable measurement performance is obtained between the BPS and BGS. Moreover, the frequency synthesized from both the BPS and BGS achieves lower measurement uncertainty.

Performance comparison

Table 1 presents a comparison of the scheme presented in this work with previously reported photonic-assisted microwave measurement methods (29, 30, 41–51). The key performance parameters for dynamic frequency identification include the instantaneous bandwidth (IBW), spectral resolution $F_{\rm res}$, frequency measurement accuracy σ , and temporal resolution $T_{\rm res}$. To compare the overall performance between different schemes, an FOM derived from these important parameters is defined, given by

$$FOM = \frac{IBW}{\sigma F_{res} T_{res}}$$
 (1)

where IBW/F_{res} reveals the maximum number of resolved frequencies, which is crucial for evaluating the performance of the system in identifying multiple frequencies. In addition, σ is calculated via the RMSE and tends to be correlated with T_{res} , as it can be enhanced by longer interaction times or increased averages. This FOM is proposed to quantify the dynamic multifrequency measurement performance and serves as a comprehensive metric. Here, note that for single-frequency measurement schemes, the maximum number of resolved frequencies is 1, i.e., $IBW/F_{res} = 1$. The comparisons reveal that the proposed scheme has the largest IBW of 50.8 GHz and a high measurement accuracy of 1.1 MHz and achieves a record FOM of 4581.82, which corresponds to a more than 10-fold enhancement in performance over those of the state-of-the-art methods. Moreover, this work reports the demonstration of amplitudemodulated signal measurements with a multifrequency detection system. Therefore, the proposed scheme with an unprecedented performance enhancement offers a groundbreaking approach for detecting and characterizing various complex microwave signals in the future.

MATERIALS AND METHODS

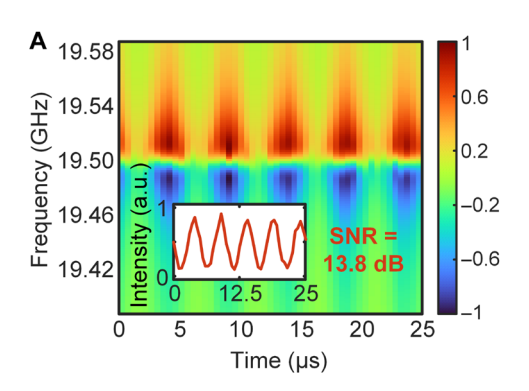
Generation of a single-sideband DOFC

Since the DOFC is generated by an AWG-driven electro-optical modulator, the amplitude and phase of each frequency component can be customized, which provides enormous flexibility. The baseband signal of the DOFC comprises multiple tone signals with a uniform frequency spacing, which is expressed as

$$e(t) = \sum_{k=1}^{N} a_k \cos\{2\pi [\nu_{\rm B} + (k-1)f_{\rm rep}]t + \varphi_k\}$$
 (2)

where the frequency comb consists of N cosine waves with a constant frequency spacing $f_{\rm rep}$ starting at an initial offset frequency $\nu_{\rm B}$, which is equivalent to the BFS of the fiber used to prevent Brillouin gain cross-talk and self-beating noise. The amplitude and phase of the kth frequency tone are denoted by a_k and ϕ_k , respectively. To implement carrier-unsuppressed single-sideband modulation, another signal with a phase difference of 90° from this baseband signal is used to codrive the DDMZM, which is manifested as a superposition of sine waves.

Because of the limitations of the device bandwidth and sampling rate, higher-frequency components suffer from more severe SNR degradation. This necessitates careful adjustment of the a_k profile to ensure frequency flatness of the received DOFC probe. By preequalizing the baseband signal, a flatter and lower noise floor across the entire modulation bandwidth can be achieved. This approach enhances the SNR of the measured Brillouin spectra, particularly for high-frequency SUT measurements. In addition, a high peak-to-average power ratio (PAPR) of the probe will result in severe nonuniform distribution of the probe power, particularly for modulations with many frequency tones. This can further deteriorate the measured Brillion spectra, hence necessitating the use of specific spectral phase encoding to control the peak power. Here, quadratic phase coding is applied to minimize the PAPR of the DOFC probes, thereby improving the SNR, i.e., $\varphi_k \propto k^2$ (52).



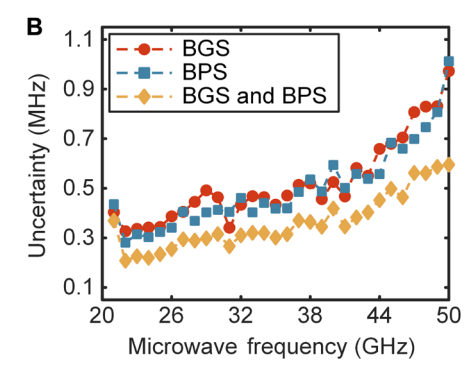


Fig. 8. Measurements based on the BPS. (A) BPS evolution of a 19.5-GHz SUT with 200-kHz sinusoidal amplitude modulation; the inset shows the measured SBS intensity variation. (B) Comparison of the measurement uncertainty with the frequencies extracted from individual BGSs, individual BPSs, and their combinations.

Scheme	IBW (GHz)	F _{res} (MHz)	σ (MHz)	T _{res}	FOM	AM measure- ment	Coverage (GHz)
(41)	16.4	-	±200	≈100 µs	0.05	×	2.3-18.7
(42)	32	-	≈755	≈3.33 ns	397.75	×	0–32
(43)	8	100	30	On the order of seconds	2.67 × 10 ⁻⁶	×	1–9
(44)	19.9	250	250	≈150 µs	2.12×10^{-3}	×	0.1–20
(29)	29	50	±1	600 μs	0.97	×	9–38
(45)	29	375	237.3 RMS	~10 ms	3.26×10^{-5}	×	1–30
(30)	7.3	10	10	500 ms	1.46×10^{-4}	×	0.3–7.6
(46)	7	40	±1	500 ms	3.5×10^{-4}	×	6–18
(47)	20	200	±100	7.3 μs	0.14	×	0–20
(48)	8	70	±3	Hundreds of milliseconds	1.79 × 10 ⁻⁵	×	1–18
(49)	20	20	±50	10 μs	2	×	1–39
(50)	3.4	100	1 RMS	100 ns	340	×	0–20
(51)	20	78	39.1 RMS	17.9 μs	0.37	×	2–22
This work	50.8	20	1.1 RMS	500 ns	4581.82		0–50.8

SBS information demodulation

A complete baseband signal consists of repeated DOFC symbols and short training symbols for synchronization. After the SBS interaction between the DOFC-modulated probe and the unknown microwave-driven pump in the fiber, the DOFC carrying the SBS information is detected by a single PD. A single sideband of the probe will beat with the optical carrier to generate a beat signal similar to the baseband signal, whose amplitude and phase are encoded by the Brillouin spectra and can be simultaneously extracted via FFT analysis. Irregular fluctuations introduced by modulation and detection always exist, leading to degradation of the demodulation. Therefore, a premeasured spectrum without SBS is needed to act as the background reference noise for channel estimation to obtain the Brillouin spectra without distortion. Last, the BGS, BLS, and BPS in the received spectrum are localized by the corresponding fitting

algorithms. The retrieved BFS and SBS intensities are then mapped to the instantaneous frequencies and amplitudes of the microwave signals, respectively.

REFERENCES AND NOTES

- X. Zou, B. Lu, W. Pan, L. Yan, A. Stöhr, J. Yao, Photonics for microwave measurements. Laser Photonics Rev. 10. 711–734 (2016).
- 2. S. Pan, Y. Zhang, Microwave photonic radars. J. Lightwave Technol. 38, 5450-5484 (2020).
- J. Capmany, D. Novak, Microwave photonics combines two worlds. Nat. Photonics 1, 319–330 (2007).
- B. Lu, W. Pan, X. Zou, H. Jiang, X. Yan, P. Li, F. Zou, L. Yan, B. Luo, Photonic-assisted intrapulse parameters measurement of complex microwave signals. *J. Lightwave Technol.* 36, 3633–3644 (2018).
- D. Zhu, S. Pan, Broadband cognitive radio enabled by photonics. J. Lightwave Technol. 38, 3076–3088 (2020)
- P. W. East, Fifty years of instantaneous frequency measurement. IET Radar Sonar Navig. 6, 112–122 (2012).

SCIENCE ADVANCES | RESEARCH ARTICLE

- R. A. Minasian, Ultra-wideband and adaptive photonic signal processing of microwave signals. IEEE J. Quantum Electron. 52, 0600813 (2016).
- 8. J. Yao, Microwave photonics. J. Lightwave Technol. 27, 314-335 (2009).
- S. Pan, J. Yao, Photonics-based broadband microwave measurement. J. Lightwave Technol. 35, 3498–3513 (2016).
- M. Pelusi, F. Luan, T. D. Vo, M. R. E. Lamont, S. J. Madden, D. A. Bulla, D. Y. Choi,
 B. Luther-Davies, B. J. Eggleton, Photonic-chip-based radio-frequency spectrum analyser with terahertz bandwidth. *Nat. Photonics* 3, 139–143 (2009).
- L. A. Bui, Recent advances in microwave photonics instantaneous frequency measurements. Prog. Quantum Electron. 69, 100237 (2019).
- H. Chi, X. Zou, J. Yao, An approach to the measurement of microwave frequency based on optical power monitoring. *IEEE Photonics Technol. Lett.* 20, 1249–1251 (2008).
- J. Li, L. Pei, T. Ning, J. Zheng, Y. Li, R. He, Measurement of instantaneous microwave frequency by optical power monitoring based on polarization interference. J. Lightwave Technol. 38, 2285–2291 (2020).
- L. V. T. Nguyen, D. B. Hunter, A photonic technique for microwave frequency measurement. *IEEE Photonics Technol. Lett.* 18, 1188–1190 (2006).
- X. Zou, S. Pan, J. Yao, Instantaneous microwave frequency measurement with improved measurement range and resolution based on simultaneous phase modulation and intensity modulation. *J. Lightwave Technol.* 27, 5314–5320 (2009).
- H. Emami, M. Ashourian, Improved dynamic range microwave photonic instantaneous frequency measurement based on four-wave mixing. IEEE Trans. Micro. Theory Tech. 62, 2462–2470 (2014).
- M. Pagani, B. Morrison, Y. Zhang, A. Casas-Bedoya, T. Aalto, M. Harjanne, M. Kapulainen, B. J. Eggleton, D. Marpaung, Low-error and broadband microwave frequency measurement in a silicon chip. *Optica* 2, 751–756 (2015).
- B. Zhu, W. Zhang, S. Pan, J. Yao, High-sensitivity instantaneous microwave frequency measurement based on a silicon photonic integrated Fano resonator. *J. Lightwave Technol.* 37, 2527–2533 (2019).
- C. Xiaoen, W. Long, L. Jingbo, C. Jianping, W. Guiling, Ultra-broadband multi-tone frequency measurement based on the recirculating frequency shift of a frequency modulated continuous wave. *Opt. Express* 32, 13864–13872 (2024).
- G. Wang, Q. Meng, Y. J. Li, X. Li, Y. Zhou, Z. Zhu, C. Gao, H. Li, S. Zhao, Photonic-assisted multiple microwave frequency measurement with improved robustness. *Opt. Lett.* 48, 1172–1175 (2023).
- T. Hao, J. Tang, N. Shi, W. Li, N. Zhu, M. Li, Multiple-frequency measurement based on a Fourier domain mode-locked optoelectronic oscillator operating around oscillation threshold. Opt. Lett. 44, 3062–3065 (2019).
- J. Shi, F. Zhang, D. Ben, S. Pan, Simultaneous radar detection and frequency measurement by broadband microwave photonic processing. *J. Lightwave Technol.* 38, 2171–2179 (2020).
- T. A. Nguyen, E. H. W. Chan, R. A. Minasian, Photonic multiple frequency measurement using a frequency shifting recirculating delay line structure. *J. Lightwave Technol.* 32, 3831–3838 (2014).
- F. Zhou, H. Chen, X. Wang, L. Zhou, J. Dong, X. Zhang, Photonic multiple microwave frequency measurement based on frequency-to-time mapping. *IEEE Photonics J.* 10, 5500807 (2018).
- D. Huang, Y. Shi, F. Li, P. K. A. Wai, Fourier domain mode locked laser and its applications. Sensors 22, 3145 (2022).
- T. Hao, Y. Liu, J. Tang, Q. Cen, W. Li, N. Zhu, Y. Dai, J. Capmany, J. Yao, M. Li, Recent advances in optoelectronic oscillators. Adv. Photonics 2, 044001 (2020).
- Y. Xiao, J. Guo, K. Wu, W. Dong, P. Qu, X. Zhang, S. Ruan, W. Chen, Multiple microwave frequencies measurement based on stimulated Brillouin scattering with improved measurement range. Opt. Express 21, 31740–31750 (2013).
- B. J. Eggleton, C. G. Poulton, P. T. Rakich, M. J. Steel, G. Bahl, Brillouin integrated photonics. Nat. Photonics 13, 664–677 (2019).
- H. Jiang, D. Marpaung, M. Pagani, K. Vu, D. Y. Choi, S. J. Madden, L. Yan, B. J. Eggleton, Wide-range, high-precision multiple microwave frequency measurement using a chip-based photonic Brillouin filter. *Optica* 3, 30–34 (2016).
- T. Shi, Y. Chen, Multiple radio frequency measurements with an improved frequency resolution based on stimulated Brillouin scattering with a reduced gain bandwidth. Opt. Lett. 46, 3460–3463 (2021).
- H. Wang, Y. Dong, High-performance transient SBS-based microwave measurement using high-chirp-rate modulation and advanced algorithms. Opt. Lett. 48, 3291–3294 (2023).
- D. Zhou, Y. Dong, B. Wang, C. Pang, D. Ba, H. Zhang, Z. Lu, H. Li, X. Bao, Single-shot BOTDA based on an optical chirp chain probe wave for distributed ultrafast measurement. *Light Sci. Appl.* 7, 32 (2018).
- 33. D. Marpaung, On-chip photonic-assisted instantaneous microwave frequency measurement system. *IEEE Photonics Technol. Lett.* **25**, 837–840 (2013).
- Z. Zhao, K. Zhu, L. Lu, C. Lu, Instantaneous microwave frequency measurement using few-mode fiber-based microwave photonic filters. Opt. Express 28, 37353–37361 (2020).

- S. Song, S. X. Chew, L. Nguyen, X. Yi, High-resolution microwave frequency measurement based on dynamic frequency-to-power mapping. Opt. Express 29, 42553–42568 (2021).
- X. Bao, Z. Zhou, Y. Wang, Review: Distributed time-domain sensors based on Brillouin scattering and FWM enhanced SBS for temperature, strain and acoustic wave detection. *Photonix* 2, 14 (2021).
- H. He, Z. Zhao, W. Wei, C. Zhao, D. Huang, M. Tang, High-accuracy sweep-free BOTDA enabled by simultaneous full-field Brillouin spectra measurement. *IEEE Sens. J.* 24, 39020–39027 (2024).
- X. Long, W. Zou, J. Chen, Broadband instantaneous frequency measurement based on stimulated Brillouin scattering. Opt. Express 25, 2206–2214 (2017).
- W. Jiao, K. You, J. Sun, Multiple microwave frequency measurement with improved resolution based on stimulated Brillouin scattering and nonlinear fitting. *IEEE Photonics J.* 11. 5500912 (2019).
- H. He, Z. Zhao, S. Fu, D. Liu, M. Tang, High spatial resolution fast Brillouin optical time-domain analysis enabled by frequency-agility digital optical frequency comb. Opt. Lett. 47, 3403–3406 (2022).
- H. Zhang, S. Pan, High resolution microwave frequency measurement using a dual-parallel Mach–Zehnder modulator. *IEEE Microw. Wireless Compon. Lett.* 23, 623–625 (2013).
- M. Burla, X. Wang, M. Li, L. Chrostowski, J. Azaña, Wideband dynamic microwave frequency identification system using a low-power ultracompact silicon photonic chip. *Nat. Commun.* 7, 13004 (2016).
- S. Zheng, S. Ge, X. Zhang, H. Chi, X. Jin, High-resolution multiple microwave frequency measurement based on stimulated Brillouin scattering. *IEEE Photonics Technol. Lett.* 24, 1115–1117 (2012).
- T. A. Nguyen, E. H. W. Chan, R. A. Minasian, Instantaneous high-resolution multiplefrequency measurement system based on frequency-to-time mapping technique. *Opt. Lett.* 39, 2419–2422 (2014).
- X. Wang, F. Zhou, D. Gao, Y. Wei, X. Xiao, S. Yu, J. Dong, X. Zhang, Wideband adaptive microwave frequency identification using an integrated silicon photonic scanning filter. *Photonics Res.* 7, 172–181 (2019).
- J. Liu, T. Shi, Y. Chen, High-accuracy multiple microwave frequency measurement with two-step accuracy improvement based on stimulated Brillouin scattering and frequency-to-time mapping. J. Lightwave Technol. 39, 2023–2032 (2021).
- B. Zhu, J. Tang, W. Zhang, S. Pan, J. Yao, Broadband instantaneous multi-frequency measurement based on a Fourier domain mode-locked laser. *IEEE Trans. Micro. Theory Tech.* 69, 4576–4583 (2021).
- L. Wang, T. Hao, M. Guan, G. Li, M. Li, N. Zhu, W. Li, Compact multi-tone microwave photonic frequency measurement based on a single modulator and frequency-to-time mapping. J. Lightwave Technol. 40, 6517–6522 (2022).
- P. Zhou, Z. Tang, J. Zhu, N. Li, Instantaneous frequency measurement using photonicsassisted broadband signal generation and processing. *IEEE Microw. Wireless Technol. Lett.* 33, 619–622 (2023).
- H. Wang, Y. Dong, Real-time and high-accuracy microwave frequency identification based on ultra-wideband optical chirp chain transient SBS effect. *Laser Photonics Rev.* 17, 2200239 (2023)
- X. Li, Z. Fan, J. Su, Y. Wang, S. Shi, Q. Qiu, Photonic-assisted wideband microwave frequency measurement based on optical heterodyne detection. *Opt. Express* 32, 18127–18138 (2024).
- M. Soriano-Amat, H. F. Martins, V. Durán, S. Martin-Lopez, M. Gonzalez-Herraez, M. R. Fernández-Ruiz, Quadratic phase coding for SNR improvement in time-expanded phase-sensitive OTDR. Opt. Lett. 46, 4406–4409 (2021).

Acknowledgments

Funding: This work was supported by National Key R&D Program of China grant 2023YFB2906303 (to Z.Z.), Major Program (JD) of Hubei Province grant 2023BAA013 (to M.T.), National Natural Science Foundation of China grants 62225110 (to M.T.) and 62105111 (to Z.Z.), Hong Kong Research Grants Council (RGC) under general research fund grants 15224521 (to A.P.T.L.) and 15212924 (to A.P.T.L.), and Project 1-CD8L of the Hong Kong Polytechnic University (to A.P.T.L.). **Author contributions:** Z.Z. conceived the study. H.H. and Z.Z. designed the methodology. H.H. and J.W. designed and conducted the experiments with assistance from D.H., A.P.T.L., and C.L. H.H. performed the data analysis. Z.Z. and M.T. supervised and coordinated the work. H.H. and Z.Z. wrote the manuscript with contributions and feedback from all coauthors. **Competing interests:** The authors declare that they have no competing interests. **Data and materials availability:** All data needed to evaluate the conclusions in the paper are present in the paper.

Submitted 11 November 2024 Accepted 26 March 2025 Published 30 April 2025 10.1126/sciadv.adu5130